Enhancing the fluorescence of individual thick shell CdSe/CdS nanocrystals by coupling to gold structures

Damien Canneson, Ikbel Mallek-Zouari, Stéphanie Buil, Xavier Quélin, Clémentine Javaux, Benoit Dubertret, Jean-Pierre Hermier

Enhancing the fluorescence of individual thick shell CdSe/CdS nanocrystals by coupling to gold structures

2012 New J. Phys. 14 063035

(http://iopscience.iop.org/1367-2630/14/6/063035)

New Journal of Physics
The open-access journal for physics

Enhancing the fluorescence of individual thick shell CdSe/CdS nanocrystals by coupling to gold structures

D Canneson[1], I Mallek-Zouari[1], S Buil[1], X Quélin[1], C Javaux[2], B Dubertret[2,4] and J-P Hermier[1,3,4]

[1] Groupe d'Études de la Matière Condensée, Université de Versailles-Saint-Quentin-en-Yvelines, CNRS UMR8635, 45, avenue des États-Unis, F-78035 Versailles, France
[2] Laboratoire de Physique et d'Étude des Matériaux, CNRS UMR8213, ESPCI, 10, rue Vauquelin, F-75231 Paris, France
[3] Institut Universitaire de France, 103, boulevard Saint-Michel, F-75005 Paris, France
E-mail: hermier@physique.uvsq.fr and benoit.dubertret@espci.fr

New Journal of Physics **14** (2012) 063035 (16pp)
Received 14 December 2011
Published 26 June 2012
Online at http://www.njp.org/
doi:10.1088/1367-2630/14/6/063035

Abstract. The fluorescence properties of individual CdSe/CdS nanocrystals (NCs) with a very thick shell and deposited on metallic structures are analyzed in detail. The results obtained for two metallic structures consisting of a continuous or a semi-continuous gold film are compared. Under low pulsed excitation, a strong acceleration of radiative processes is observed. The probability of electron–hole pair recombinations through Auger processes dramatically decreases, resulting in a suppression of blinking and the appearance of biexcitonic cascades. An original method of photons postselection also enables us to determine the decay rate corresponding to biexcitonic recombinations. Finally, a detailed analysis of the excitation process and the photon collection efficiency enables us to discriminate the effect of the gold structure in terms of excitation and fluorescence acceleration. It is found that high collection percentages can be achieved through the modification of NC emission with plasmonic structures.

[4] Authors to whom any correspondence should be addressed.

Contents

1. Introduction

The effects of metallic surfaces on fluorescence have been studied since 1968 when Drexhage first reported the possibility of modifying the spontaneous emission of Eu^{3+} ions by locating them close to a silver film [1]. More recently, the interactions of fluorophores with metallic structures were used in biology to increase intensities of fluorescence but also to design detection systems based on fluorescence quenching [2, 3].

Developments in the field of plasmonics also open up the possibility of controlling the emission of a single emitter for the generation of quantum states of light such as single photons [4–8]. The radiation pattern of the emitter is modified by its coupling with the structure, and a better collection efficiency can be achieved [9]. The spontaneous decay rate can also be increased through the Purcell effect [10] that is quantified by the Purcell factor F_P. For an emitter coupled to a cavity, with a linewidth narrower than the spectral width of the cavity mode, the Purcell factor is proportional to Q/V, where V is the volume of the electromagnetic mode and Q its quality factor. With the dielectric nanocavities such as micropillars [11], microdiscs [12] or photonic crystals [13] exhibiting quality factors greater than thousands, Purcell factors greater than 10 have been obtained.

In the visible range of the electromagnetic spectrum, losses make the quality factor of metallic nanocavities lower than that of dielectric ones. But the spatial confinement of the electromagnetic field is much higher. Even if the volume V cannot be rigorously defined as for dielectric cavities [14], a strong spatial localization of the electromagnetic field is achieved with the metallic nanostructures. The volume V can be much lower than the cube of the wavelength that is the limiting value for dielectric cavities.

Moreover, metallic structures are especially suited for emitters operating at room temperature, such as colloidal nanocrystals (NCs), since they present a rather large linewidth (for a standard NC, the typical quality factor of the emitter is $Q_e \sim 20$ at $\lambda = 660$ nm). Indeed, when Q_e is lower than Q, there is no gain sharpening the resonance of the cavity. In a general way, the use of metallic structures gives the opportunity for developing devices exhibiting a

very broad bandwidth that increases the accordability of the cavity with the emission of the fluorophore [15]. Several groups are now involved in the control of a single NC fluorescence with a metallic nanostructure [16–19].

Due to losses in a metal, it is also difficult to predict whether the coupling of a nano-emitter with a metallic structure, such as a nanoparticle, a rough or a continuous surface, will quench or enhance fluorescence [20]. In the case of standard CdSe/ZnS NCs [17, 18], quenching is often observed. Electron transfers between the NC and the metal are not prevented by the thin shell (about 1 atomic layer) of these core/shell structures as well as the excitation of lossy modes. In this paper, the opportunities opened by a new type of colloidal semiconductor NCs are investigated. Recently, two groups succeeded in synthesizing core/shell structures consisting of a CdSe core and a very thick and crystalline shell ($\geqslant$5 nm) of CdS [21, 22]. These core/shell NCs exhibit very low blinking. The duration of low emitting periods never exceeds 50 ms, in sharp contrast with standard CdSe/ZnS NCs [23]. Moreover, these periods are not completely dark as for CdSe/ZnS NCs but correspond to a gray state with a quantum efficiency (QE) at least of the order of 20% [24]. When they are coupled to metallic structures, the following results show that the thick shell provides an intrinsic spacer between the emitter and the metal that avoids the quenching of the fluorescence.

Here, the coupling of single CdSe/CdS NCs deposited directly on a continuous or a semi-continuous gold film is studied in detail. In comparison with many previous experiments [7, 17, 18, 25], the improvements induced by the metallic structure in terms of excitation and increase of the fluorescence decay of the NC are distinguished. Moreover, a detailed assessment of the radiative and non-radiative channels opened by the coupling between the NCs and the gold structures is provided. For a low optical excitation, we characterize the photoluminescence (PL) decay and the time statistic of the photons emitted by individual NCs with original methods. An analysis of the excitation process under pulsed excitation provides the contribution of the excitation enhancement near the metal film. The coupling between the NC and the gold structure results in a strong enhancement of the fluorescence, corresponding to F_P values up to 60. The blinking suppression is also observed. The histogram of the intensity shows that this suppression corresponds to a strong reduction of Auger recombinations. By using second-order autocorrelation function measurements, we show that this reduction also leads to very efficient biexcitonic cascades. The data concerning the time detection of the photons also enable us to determine the PL decay corresponding to the recombinations of biexcitons. Finally, a precise analysis of the excitation process and the rate of collected photons is performed. It is shown that a high efficiency of the photon collection and a strong reduction of the excited state lifetime can be simultaneously achieved.

2. Experimental setup

The CdSe/CdS NCs ($\lambda = 660$ nm with a full-width at half-maximum of 32 nm) are core/shell structures composed of a CdSe core (3 nm radius) and a thick crystalline shell of CdS (7 nm, rms $\sim$1 nm). Their synthesis is presented in detail in [21]. In quasi-type II CdSe/CdS NCs, the electron is partially delocalized in the shell. The overlap between the electron and hole wavefunctions is reduced, resulting first in an increase of the radiative and Auger lifetimes. In contrast with standard CdSe/ZnS NCs, the fluorescence of ionized CdSe/CdS NCs is not quenched by Auger recombination. Under low power pulsed excitation, when the probability of generating one electron–hole (e–h) pair per pulse is much higher than the probability of

creating several ones, CdSe/CdS NCs oscillate between two states: a bright state corresponding to a monoexciton (denoted as X) that always recombines radiatively ($QE_X = 100\%$ [24]), and a gray state for a trion (denoted as X^*) that decays with a lower radiative QE.

The gold film is prepared by evaporation under ultra-high vacuum (10^{-9} torr). By adjusting the duration of deposition, a semi-continuous film just below the percolation threshold [26–28] or a continuous film can be obtained. The standard continuous and flat film presents a thickness of 20 nm and a roughness of 0.8 nm (rms, AFM measurements). The properties of its delocalized plasmon modes have been widely studied [29]. For the semi-continuous gold film, a wide distribution of plasmon resonances has been observed. Their spectrum covers the visible range above 550 nm [30] and includes the wavelength emission ($\lambda = 660$ nm) of the NCs. In sharp contrast with the continuous film, these disordered nanostructures also exhibit high localization of plasmon modes. The electromagnetic energy confinement in subwavelength-sized regions called 'hot spots' [26, 28, 31] has been identified. Strong intensities are theoretically predicted and experimentally observed [30]. More recently, these localized plasmon resonances have also been studied through the fluctuations of the local density of optical states [32].

The NCs are suspended in a mixture of 90% hexane and 10% octane and spin coated in such a way that individual NCs could be observed with an epifluorescent microscope (IX 71, Olympus). The NCs are excited by a pulsed laser diode emitting at 485 nm (LDH 485, Picoquant, pulse duration $\leqslant$100 ps). Their fluorescence is collected through an air objective with a numerical aperture (NA) of 0.95 and sent into a Hanbury-Brown and Twiss setup presenting a high sensitivity (avalanche photodiodes MPD; time resolution of 50 ps). The photodetection signals were analyzed by a PicoHarp 300 module (Picoquant). For each photon, an internal clock (with a click every 50 ns) records the absolute time of arrival with respect to the beginning of the whole measurement. The card also records the delay between the photons and the laser pulse (64 ps accuracy). Since there is no drift between the laser diode and the internal clock of the module, the addition of the two times provides the absolute time of arrival of each photon with a precision limited by a time resolution of 64 ps. The time evolution of the fluorescence intensity, the second-order autocorrelation function and the PL decay can be extracted from these data. Moreover, when biexcitonic cascades are observed, in contrast with a standard setup that only records the delay between photons, the setup enables us to distinguish unambiguously the photons stemming from the emissions of the biexciton or of the monoexciton.

3. Results

3.1. Preliminary results

First of all, the emission of individual NCs spin coated on a glass coverslip (oil objective, NA = 1.4) under low-power excitation is recorded. The fluorescence intensity of a single NC switches between two values corresponding to the bright (X) and the gray (X^*) states (figure 1). As in [24], perfect antibunching (data not shown) was always observed, showing that the NCs are individual. The histogram of the intensity shows two bumps denoted as A and B with areas proportional to the probability occurrence of the bright and gray states. The relative positions of the A and B bumps in figure 1(b) correspond, respectively, to the mean intensity of X^* and X states. They are proportional to the radiative QE of each state. Since the QE of the bright state QE_X is 100%, $QE_{X^*} = 40\%$ is calculated [24]. The total PL decay is well adjusted by a bi-exponential decay function (figure 1(c)). The short component is the charged exciton (X^*)

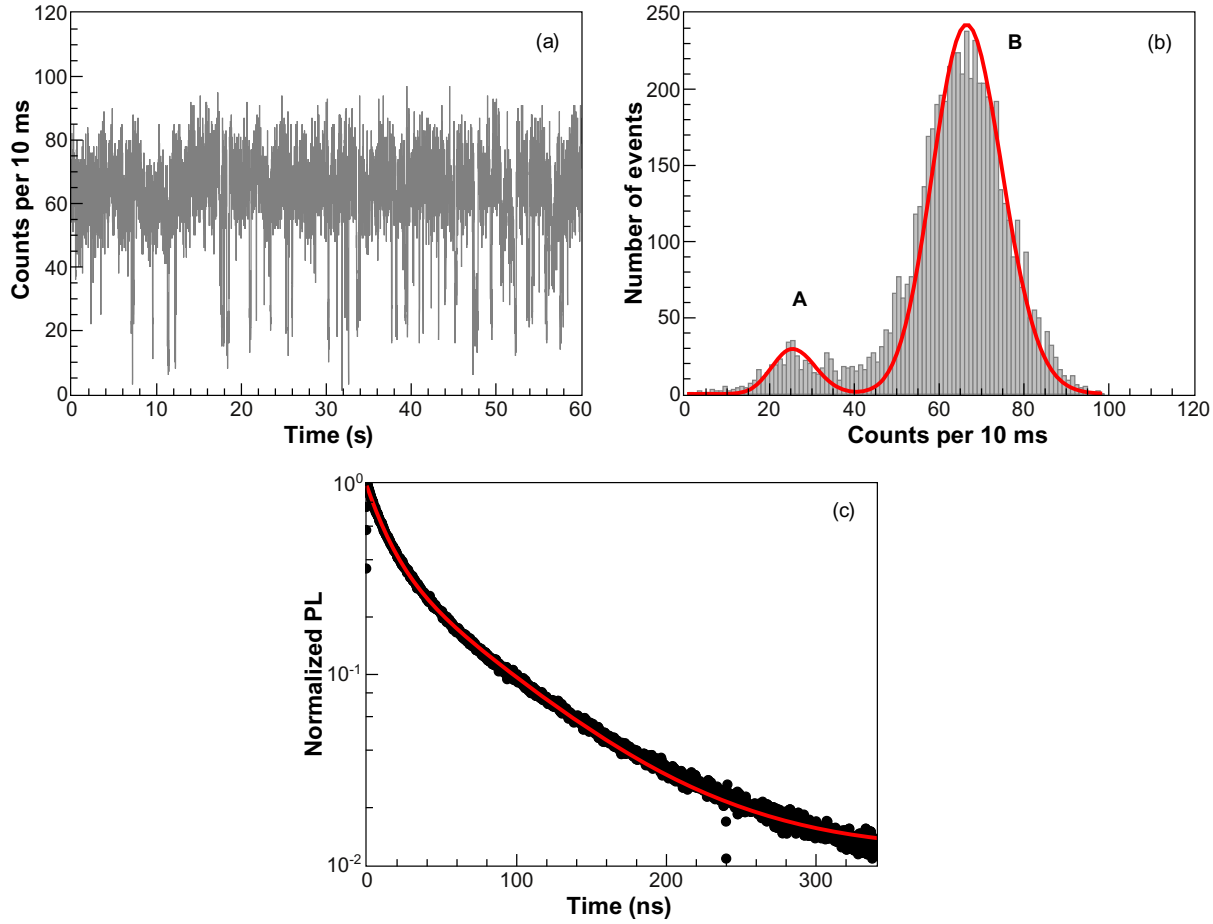

Figure 1. (a) Fluorescence intensity of a single CdSe/CdS NC on a glass coverslip (time binning $t_b = 10$ ms). (b) Intensity histogram corresponding to panel (a). (c) PL decay of the fluorescence. The red line is a bi-exponential fit (with an offset; lifetimes of 13 and 65 ns).

lifetime (13 ns), while the long component (65 ns) is the monoexciton (X) lifetime. From the procedure described in [24], the Auger lifetime (∼20 ns) and the radiative lifetime (∼30 ns) of the X* state are deduced. These values are slightly higher than those reported in [24] owing to the thicker shell of the NC used here. They will be used as references in the following.

For a further precise determination of the collection efficiency on gold films, the probability of excitation with the air objective is now to be determined. First, the emission of individual NCs spin coated on a glass coverslip is analyzed. At saturation, for a repetition rate of 5 MHz, the intensity I_{sat} is equal to 20 kHz, i.e. 0.4% of the laser pulses generate a photon detected by the optical setup. In the following experiments, the laser power is set to a constant value. For the glass coverslip, the pump power μ_{Glass} then corresponds to a fluorescence intensity equal to 6 kHz (30% of I_{sat}). The probability $P(n)$ to generate n e–h pairs per pulse follows a Poissonian statistics [24], $P(n) = \eta^n \exp(-\eta)/n!$ (η is the mean of the distribution). From the value $\sum_1^\infty P(n) = 30\%$, $\eta_{Glass} = 36\%$, $P(1) = 25\%$ and $P(2) = 4.5\%$ are calculated. The probability of exciting several e–h pairs is more than 5 times lower than the probability of exciting only one, which means that NCs are operating in a low excitation regime. In order

Table 1. The mean number η of e–h pairs created per pulse and probabilities $P(n)$ for the different configurations.

Configuration	Pump	η (%)	$P(1)$ (%)	$P(2)$ (%)
Glass coverslip	μ_{Glass}	36	25	4.5
Continuous film	μ_{CF}	48	30	7.2
Semi-continuous film	μ_{SCF}	40	27	5.4

to precisely calculate the excitation probability of a NC when coupled to one of the gold films, the reflectivity of each film at the excitation wavelength of 485 nm has to be taken into account (in a previous paper [33], the probability of excitation was lower and the effect of the gold film reflectivity could be neglected). Spectrophotometric measurements give $R = 13\%$ for the semi-continuous film and $R = 35\%$ for the continuous gold film. The pump power μ_{CF} can be assumed to be equal to $\mu_{\text{CF}} = 1.35 \times \mu_{\text{Glass}}$. Concerning the semi-continuous film, an important point is that no plasmon can be excited at 485 nm and the fluctuations of the near-field intensity at this wavelength due to the metallic pattern are lower than 10% [30]. So, the pump power is considered to be homogeneous on the surface and equal to $\mu_{\text{SCF}} = 1.13 \times \mu_{\text{Glass}}$. In table 1, we summarize the pump power for the different configurations, the mean number η of e–h pairs created and the corresponding probabilities $P(n)$. The control of the excitation power will be a key point to infer the collection efficiency of the photons. In the following, the contribution of biexcitonic cascades to the total fluorescence intensity will also be evaluated.

3.2. Photoluminescence decay

In this section, the PL decay acceleration is compared on continuous and semi-continuous films. Figure 2(a) shows the PL decay measurements for four NCs directly deposited on the continuous film. They can be fitted by a bi-exponential decay function. As in the case of a glass coverslip, the long component is interpreted as the lifetime of X, while the short one is that of X* (in the following, we will see that a low percentage of the short component also corresponds to biexcitonic emission). As expected, the lifetimes of X and X* (see table 2) do not also depend on the NC (the PL decay of NC_d is faster since it spends more time in the ionized state). The Purcell factor for the bright state is close to 6, a value that is consistent with theoretical predictions [3]. For the semi-continuous gold film, due to the strong localization and exaltation of the intensity characterizing the plasmons, the PL decay is much faster than that in the case of the continuous film (figure 2(b)). The Purcell factor can reach values as high as 60. For NC2, NC3 and NC4, the time resolution of the experiment (∼150 ps) does not allow us to distinguish the PL decay of X and X*. The data's adjustment only provides an approximate value of the X lifetime (see table 2). Moreover, the decay rate depends on the NC considered. This feature can be attributed to the very specific plasmon modes on the disordered gold film. Localized at the nanometer scale, they exhibit random spatial localization which induces strong fluctuations in the local density of states already observed through a modification of the fluorescence of polystyrene beads [32].

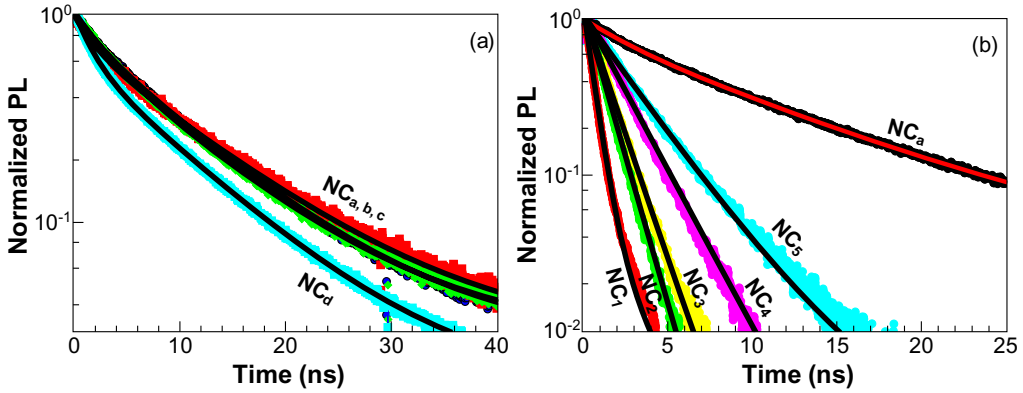

Figure 2. (a) PL decay of four NCs deposited on the continuous film (NC_a, NC_b, NC_c and NC_d). (b) PL decay of five NCs deposited on the semi-continuous film (NC_1, NC_2, NC_3, NC_4 and NC_5), illustrating the range of decay rates. The PL decay of NC_a for the same range is also plotted for comparison.

Table 2. X, X* lifetimes and the Purcell factor (for the bright state X) of the nine NCs corresponding to figure 2. The row 'Glass coverslip' corresponds to the mean results obtained for NCs deposited on a glass coverslip. For NC_2, NC_3 and NC_4 deposited on the semi-continuous film, lifetimes are too short to distinguish the two components.

		τ_X (ns)	τ_{X^*} (ns)	F_P (X)
Glass coverslip		65	13	
Continuous film	NC_a	11	2	5.9
	NC_b	10	3	6.5
	NC_c	10	2.5	6.5
	NC_d	9.3	1.7	7
Semi-continuous film	NC_1	2	0.6	33
	NC_2	1.1		∼60
	NC_3	1.3		∼50
	NC_4	2.1		∼30
	NC_5	4	2.6	16

3.3. Fluorescence intensity

Next, the difference in fluorescence intensity between the continuous and semi-continuous films is analyzed. In both cases, the very thick shell of the NCs minimizes the generation of lossy surface waves and prevents the fluorescence quenching of the NCs coupled to the continuous or semi-continuous gold films. Figure 3(a) presents the results obtained for a NC coupled to the semi-continuous film. No blinking is observed. The histogram of the intensity (figure 3(b)) is perfectly fitted by a Poissonian distribution corresponding to the fluctuations observed for a single emitting state. The radiative recombinations have become so fast that Auger recombination of the X* is prevented. The radiative efficiency of the trion state is then equal to that of the neutral state.

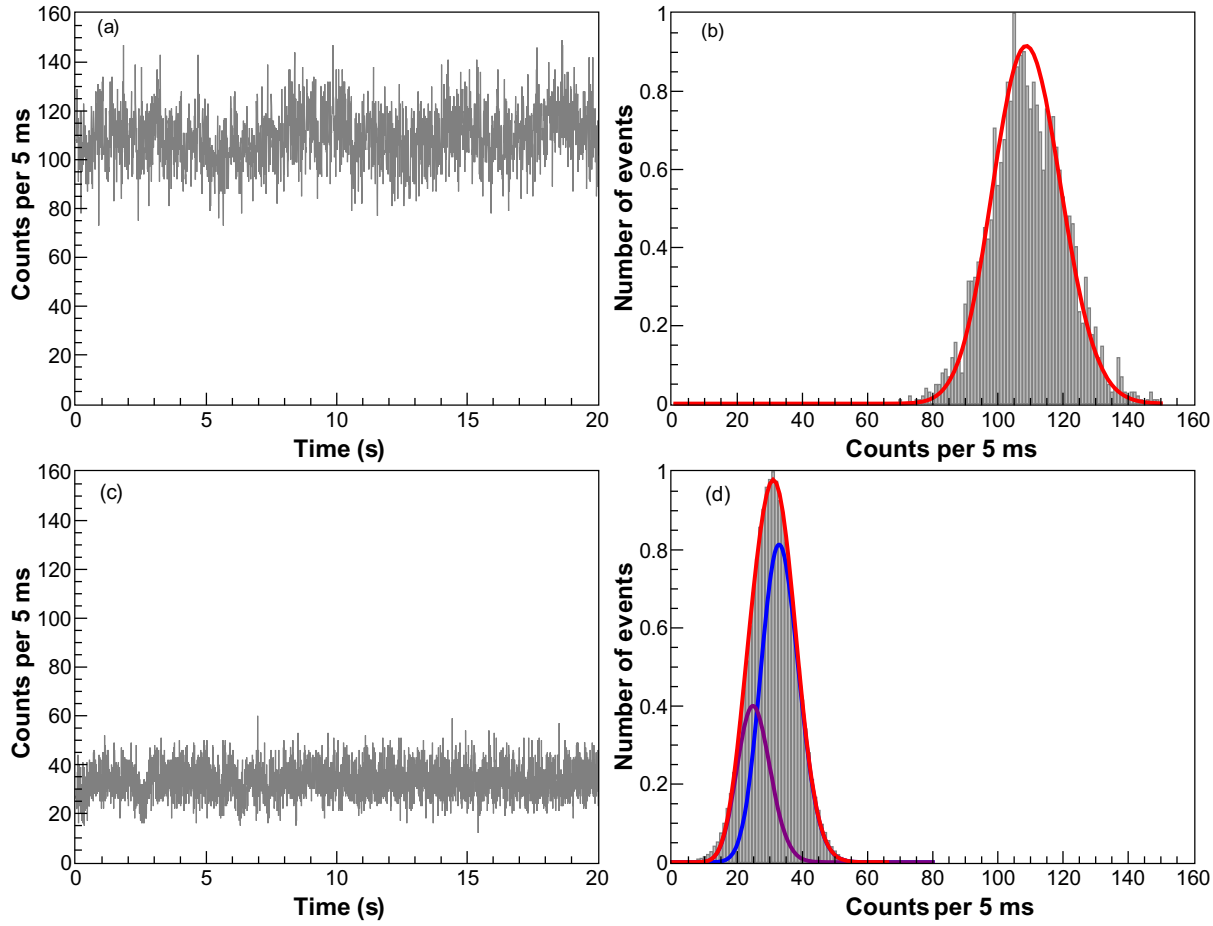

Figure 3. (a) Fluorescence intensity of a NC deposited on the semi-continuous film (zoom on 20 s; $t_b = 5$ ms). (b) Intensity histogram corresponding to panel (a). The bars represent the experimental results. The red line is a Poissonian distribution fit (mean value of 109). (c) Fluorescence intensity of a NC deposited on the continuous film (zoom on 20 s; $t_b = 5$ ms). (d) Intensity histogram corresponding to panel (c). The bars represent the experimental results. The red line is a fit corresponding to the sum of two Poissonian distributions (violet and blue lines; mean values of 25 and 33).

The histogram of the intensity of a NC coupled to the continuous film (figure 3(d)) is not fitted well by a Poissonian distribution but can be numerically fitted by the sum of two Poissonian distributions corresponding to the intensity fluctuations of the ionized and neutral states (the emission for these two states can be considered as independent processes, so we can add the two Poissonian distributions). The acceleration of the radiative recombination of the trion is lower than that in the case of a semi-continuous film. Auger recombinations can still occur and the QE of X^* is lower than the QE of X. From the mean value of the two Poissonian distributions, $QE_{X^*} = 0.76 \times QE_X$ is deduced.

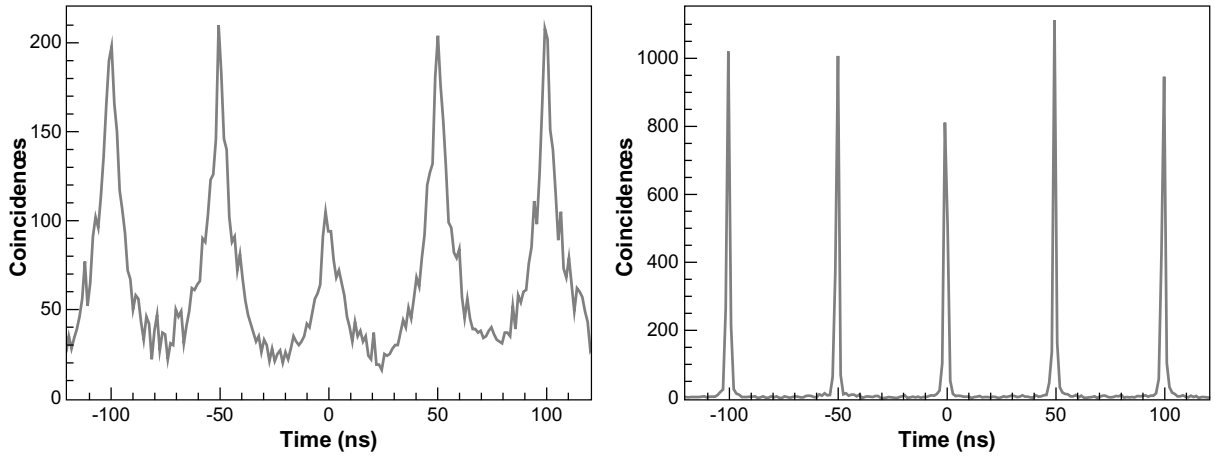

Figure 4. Coincidence counts for a NC deposited on the continuous (a) and semi-continuous (b) films.

3.4. Autocorrelation of the intensity

The suppression of blinking under low-power excitation comes from the enhancement of radiative processes. In the case of the semi-continuous film, the radiative recombination of X^* is so fast that Auger recombination can be completely neglected. The Auger processes also being at the very origin of the single-photon emission in colloidal NCs, the consequences of increasing the radiative decay rate are now studied from the point of view of the quantum properties of NC emission. Figure 4(a) shows the histogram of delays between photons for a NC deposited on the continuous gold film. The antibunching is still observed but the presence of a peak at zero delay is evidence that radiative recombination of the neutral (XX) or charged (XX^*) biexcitonic states occurs. The QE of the biexcitonic emission is now analyzed by using a method based on the intensity autocorrelation measurement (it is presented in detail in [36]). The area of the peak at zero delay is about 50% of the mean area of the lateral peaks. Under low excitation, this value is the ratio between the mean radiative QE of the biexcitonic emission and the mean radiative QE of the monoexcitonic one (X and X^* present very close QEs and we assume that XX and XX^* QEs are also very close).

When a semi-continuous film is used as metallic structure (figure 4(b)), Auger recombination of the XX and XX^* states can be completely neglected. The peak at zero delay has the same area as the other ones; the NC is no longer a single-photon emitter. This also shows that the biexcitonic and monoexcitonic states are characterized by the same coupling to the semi-continuous film. Due to the spectral width of its plasmon mode ($\geqslant$30 nm), the gold film can be considered as a photonic system with a large bandwidth that includes all the radiative processes involved in the NC de-excitation.

3.5. Postselection of the photons: measurement of the decay rate of the biexciton for a nanocrystal deposited on the semi-continuous film

Under low-power excitation, the probability of generating two photons is much lower than the probability of generating one ($P(2)/P(1)$ ranges between 0.18 and 0.26). Moreover, in the case of the semi-continuous film, XX and XX^* states recombine on a very short time scale, like the

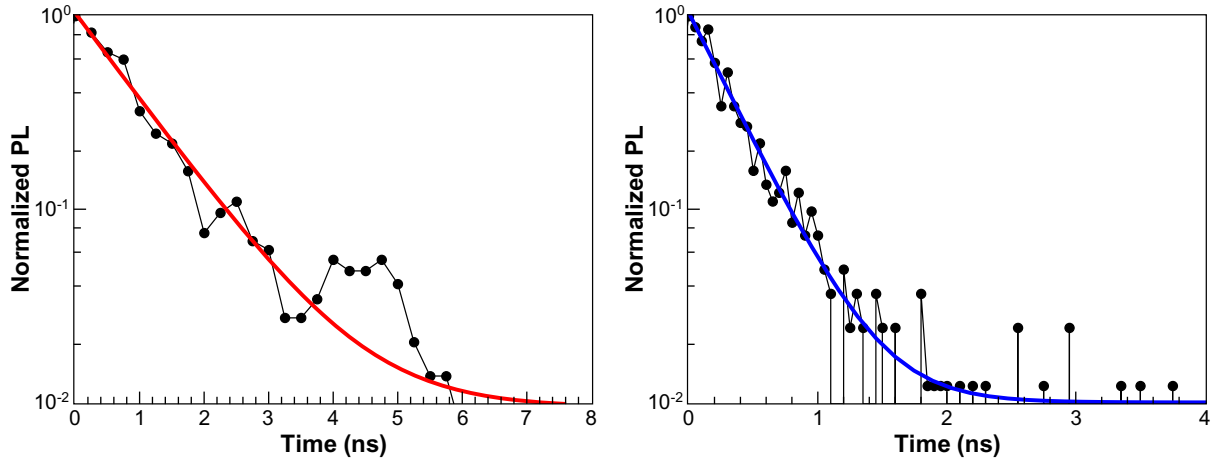

Figure 5. (a) PL decay of X* states. The red line is a monoexponential decay (with an offset, lifetime of 0.96 ns). (b) PL decay of XX* states. The blue line is a monoexponential decay (with an offset, lifetime of 0.32 ns).

X* state. A precise determination of the decay rate of the biexcitonic states through the fit of the PL decay with a multiexponential distribution is not possible. To circumvent this difficulty, an original method based on the autocorrelation measurements is now presented. In the peak at delays close to zero (figure 4(a)), coincidences correspond to the detection of a two-photon cascade. The first photon is due to the radiative recombination of XX or XX*, while the second photon corresponds to X or X* de-excitation. Since the delay between the laser pulse and each collected photon is recorded, we are able to identify unambiguously the photons stemming from biexciton recombinations and those stemming from the monoexciton recombinations and to plot the PL decay for each kind of state. Figure 5 presents the results obtained for a NC whose PL decay has a short component of 0.48 ns and a long component of 2.6 ns. Since the normalized amplitude of the short component is about 20 times higher than the amplitude of the long one, the NC is mostly ionized. X and XX emission can be neglected with a very good approximation in this case. In figure 5(a) (respectively figure 5(b)), the PL decay corresponding to X* recombination is represented (respectively XX*) after the postselection of the photons corresponding to the peak at zero delay. As expected, biexcitonic recombinations occur very fast (lifetime = 0.33 ns), on a time scale close to the resolution of the experiment. A decay of 0.96 ns is found for the monoexcitonic recombination, on the sub-ns time scale. From these data, a lifetime of 0.96 ns can be assumed for X* (the long component of 2.6 ns present in the total PL decay of figure 5(a) and corresponding to X recombination is too weak to be evidenced in the filtered signal). For this NC that is mostly ionized, the postselection method thus provides information on the emission at a very short time scale and the biexcitonic emission from the X* emission can be precisely discriminated. When the NC spends time in both states (neutral and ionized), the method provides the order of magnitude of the XX and XX* decay rates.

From a general point of view, the absence of drift between the laser and the data acquisition card enables us to know the absolute time of arrival for each photon and to calculate the autocorrelation function of the intensity, the PL decay or the variations of the intensity. Since all functions of interest are extracted from the same set of data, postselection methods can be applied very efficiently. This is very general and could be applied to other fluorophores.

3.6. Collection efficiency

In this section, the collection efficiency is properly estimated. The intensity histogram is now used to make a precise assessment of the radiative and non-radiative processes leading to the de-excitation of the X state. In contrast with dielectric structures, the coupling between an emitter and a metallic structure may result in the opening of a large number of non-radiative channels and in the suppression of the fluorescence. The acceleration of the decay is then useless. The relative importance of the radiative and non-radiative channels depends crucially on the distance between the fluorophore and the metal. The distance between the metal and the emitter can be controlled through various approaches such as the use of a silica spacer [33] or biomolecules [34]. Through a detailed analysis of the collection efficiency of the photons, the crucial role of the thick shell of the NC as a spacer can be proved. From histograms such as those of figure 3, the intensities of the X state emission can be deduced for both the continuous film and the semi-continuous film. The results obtained for all the NCs considered in figure 2 are presented in table 3. For a NC on a glass coverslip (the 'Reference' line), the intensity is 2 kHz (laser repetition rate = 5 MHz) and corresponds to a collection efficiency of the objective $\chi_{\text{obj}}^{\text{Glass}} = 20\%$ [35]. In order to calculate the collection for the gold structures, the intensity has to be corrected by taking into account the modification of the NC excitation for each structure and the QE of biexcitonic emission. For a low excitation, the collected intensity can be written as follows (see the appendices for the detailed demonstration):

- Glass coverslip: $I_{\text{tot}} = [P(1) + P(2)] \times Q_{\text{X}} \times (T \times \chi_{\text{obj}}^{\text{Glass}}) \times N$
- Continuous gold film: $I_{\text{tot}} = \left[P(1) + \frac{3}{2} \times P(2)\right] \times Q_{\text{X}} \times (T \times \chi_{\text{obj}}^{\text{CF}}) \times N$
- Semi-continuous gold film: $I_{\text{tot}} = [P(1) + 2 \times P(2)] \times Q_{\text{X}} \times (T \times \chi_{\text{obj}}^{\text{SCF}}) \times N$

where

- $\chi_{\text{obj}}^{\text{CF}}$ (respectively $\chi_{\text{obj}}^{\text{SCF}}$) is the percentage of photons collected by the objective for the continuous (respectively semi-continuous) film,
- T is the transmission of the setup except the objective,
- N is the repetition rate of the laser diode,
- Q_{X} is the radiative QE of X.

$Q_{\text{X}} \times \chi_{\text{obj}}$ represents the percentage F_{coll} of pulses leading to a photon that is collected by the objective. This value can be calculated by dividing the collected intensity by $T \times N$ and by

- $P(1) + \frac{3}{2}P(2) = 0.41$ for the continuous film,
- $P(1) + 2 \times P(2) = 0.38$ for the semi-continuous film.

For the glass coverslip, $Q_{\text{X}} = 100\%$, $\chi_{\text{obj}}^{\text{Glass}} = 20\%$ and $F_{\text{coll}} = Q_{\text{X}} \times \chi_{\text{obj}}^{\text{Glass}} = 20\%$. For the continuous and semi-continuous films, Q_{X} and χ_{obj} cannot be known independently; only F_{coll} can be evaluated. The radiative and non-radiative channels are characterized by $k_{\text{rad,coll}}$ and k_{other}. $k_{\text{rad,coll}}$ is the decay rate of processes leading to the photons emitted in the far field and collected by the objective and k_{other} is the decay rate corresponding to all the other processes: photons not collected, non-radiative recombinations, plasmons which are not coupled to the far field. Since $k_{\text{tot}} = k_{\text{rad,coll}} + k_{\text{other}}$ and $F_{\text{coll}} = k_{\text{rad,coll}}/(k_{\text{rad,coll}} + k_{\text{other}})$, $k_{\text{rad,coll}}$ and k_{other} can be calculated. If we consider the NC1, the intensity is equal to 28×10^3 counts s^{-1} and the total decay

Table 3. X lifetime and decay rates of the nine NCs corresponding to figure 2. The row 'Glass coverslip' corresponds to the mean results obtained for NCs deposited on a glass coverslip.

		I (kHz)	X lifetime (ns)	F_{coll} (%)	$k_{rad,coll}$ (MHz)	k_{other} (MHz)
Glass coverslip		6	65	20	3.1	12.3
Continuous film	NC_a	7	11	4.3	3.9	87
	NC_b	6	10	3.7	3.7	96
	NC_c	8	10	4.9	4.9	95
	NC_d	7	9.3	4.3	4.6	103
Semi-continuous film	NC_1	28	2	19	93	410
	NC_2	23	1.1	15	140	770
	NC_3	9	1.3	6	46	720
	NC_4	22	2.1	15	69	410
	NC_5	20	4	13	33	220

rate $k_{tot} = 1/2\,ns^{-1} = 500\,MHz$. Taking into account the pulse rate 20 MHz, the transmission $T = 2\%$ and $P(1) + 2 \times P(2) = 0.38$, a fraction of collected photons $k_{rad,coll}/(k_{rad,coll} + k_{other})$ equal to $28 \times 10^3/(20 \times 10^6 \times 0.02 \times 0.38) = 0.19$ is calculated. From this fraction and the total decay rate, the values $k_{rad,coll} = 93\,MHz$ and $k_{other} = 410\,MHz$ are deduced.

In the case of continuous films, the fraction of radiative processes is relatively low. Indeed, the surface plasmon excited by the NC cannot be coupled to the far field. Most of the exciton recombinations are then non-radiative. In sharp contrast with this result, a NC coupled to the semi-continuous gold film may present a collection efficiency of photons F_{coll} equal to that of a NC on a glass coverslip. The plasmons excited by the NC can be coupled to the far field due to the random structure of the film. The percentage of collected photons then depends strongly on the NC position. A crucial result is that whatever the gold structure or the position of the NC, its fluorescence is never quenched. In contrast with the results reported in previous works [9, 33], there is no need of a silica spacer between the NC and the gold structure to prevent energy transfer. In [9], standard CdSe/ZnS NCs of shell thickness lower than 1 nm were used, while in [33], CdSe/CdS with a shell of about 5 nm were used. In this work, even though most decay rates are still non-radiative, the NCs (shell thickness = 7 nm) can be detected at the single emitter level. All these results show that a size of the shell layer of about 10 nm provides an intrinsic and very efficient spacer to this kind of semiconductor quantum dot.

4. Conclusion

In conclusion, the fluorescence of individual CdSe/CdS NCs with a very thick shell and directly deposited on metallic structures has been studied in detail. A comparison of the results obtained for a continuous film and for a semi-continuous film allowed us to illustrate the changes in classical and quantum properties of the emission of the NCs. Strong Purcell effects are observed that result in a dramatic reduction of the efficiency of Auger processes. As a consequence, the blinking is suppressed and radiative recombinations of biexcitonic states occur. Through the control of the excitation, we also show that a very large collection efficiency can be achieved. In

the field of quantum plasmonics, this paper highlights the great interest of associating metallic structures and NCs, with a thick shell playing the role of a spacer. It also presents several original data analyses which could be used to study the emission of other fluorophores.

Acknowledgments

BD and J-PH acknowledge the Région Ile de France, Agence nationale de la recherche and Institut Universitaire de France for funding.

Appendix

Here the formula of the emission intensity used in section 3.6 is demonstrated. Due to the low excitation, only the generation of one e–h pair and two e–h pairs per single pulse has to be considered. In what follows, note that:

- χ_{obj} is the fraction of photons collected by the objective. It depends on the configuration (glass coverslip, continuous film (CF) or semi-continuous film (SCF)) through the radiative pattern of the NC.
- T is the transmission of the setup except the objective.
- N is the repetition rate of the laser diode.
- Q_{X} is the radiative QE of X.

A.1. Monoexcitonic excitation

The probability that a pulse generates one e–h pair is denoted as $P(1)$. The corresponding intensity is

$$I_1 = P(1) \times Q_{\mathrm{X}} \times (T \times \chi_{\mathrm{obj}}) \times N. \tag{A.1}$$

A.2. Biexcitonic excitation

When two e–h pairs are excited by a single pulse, several recombination processes have to be considered:

- The two e–h pairs recombine radiatively. The probability of this event is $Q_{\mathrm{X}} \times Q_{\mathrm{XX}}$. The probability that the two photons are detected is $(T \times \chi_{\mathrm{obj}})^2$. So we can neglect this correction. The probability that only one photon is detected is $2 \times (T \times \chi_{\mathrm{obj}}) \times \left[1 - (T \times \chi_{\mathrm{obj}})\right]$. The corresponding intensity is

  $$I_{2a} = P(2) \times Q_{\mathrm{X}} \times Q_{\mathrm{XX}} \times \left[2 \times (T \times \chi_{\mathrm{obj}})^2 + 2 \times (T \times \chi_{\mathrm{obj}}) \left[1 - (T \times \chi_{\mathrm{obj}})\right]\right] \times N. \tag{A.2}$$

- Only the biexcitonic state recombines radiatively. The probability of detecting the photon is

  $$I_{2b} = P(2) \times Q_{\mathrm{XX}} \times (1 - Q_X) \times (T \times \chi_{\mathrm{obj}}) \times N. \tag{A.3}$$

- The monoexcitonic state recombines radiatively. The probability of detecting the photon is

  $$I_{2c} = P(2) \times Q_{\mathrm{X}} \times (1 - Q_{\mathrm{XX}}) \times (T \times \chi_{\mathrm{obj}}) \times N. \tag{A.4}$$

A.3. Total intensity

The total intensity is obtained by adding the contributions of the different decay processes. A straightforward calculation gives

$$\begin{aligned} I_{\text{tot}} &= P(1) \times Q_{\text{X}} \times (T \times \chi_{\text{obj}}) \times N + P(2) \times \big[Q_{\text{X}} \times (1 - Q_{\text{XX}}) \times (T \times \chi_{\text{obj}}) \\ &\quad + Q_{\text{XX}} \times (1 - Q_{\text{X}}) \times (T \times \chi_{\text{obj}}) Q_{\text{X}} \times Q_{\text{XX}} \big[2 \times (T \times \chi_{\text{obj}})^2 \\ &\quad + 2 \times (T \times \chi_{\text{obj}}) \big[1 - (T \times \chi_{\text{obj}})\big]\big]\big] \times N \\ &= P(1) \times Q_{\text{X}} \times (T \times \chi_{\text{obj}}) \times N + P(2) \times [Q_{\text{X}} + Q_{\text{XX}}] \times (T \times \chi_{\text{obj}}) \times N \\ &= [(P(1) + P(2)) \times Q_{\text{X}} + P(2) \times Q_{\text{XX}}] \times (T \times \chi_{\text{obj}}) \times N. \end{aligned} \tag{A.5}$$

The interpretation of this equation is straightforward: the contribution of the monoexcitonic X and biexcitonic XX states to the total intensity is proportional to the probability of generating the state by one laser pulse multiplied by its radiative QE.

This equation can be simplified by considering the value of Q_{XX} with respect to Q_{X}, obtained through the area of the peak at zero delay of the autocorrelation function. One obtains

- Glass coverslip
  In this case, $Q_{\text{XX}} = 0$, which leads to

$$I_{\text{tot}} = [P(1) + P(2)] \times Q_{\text{X}} \times (T \times \chi_{\text{obj}}^{\text{Glass}}) \times N. \tag{A.6}$$

- Continuous gold film
  In this case, $Q_{\text{XX}} = \frac{1}{2} Q_{\text{X}}$, which leads to

$$I_{\text{tot}} = \big[P(1) + \tfrac{3}{2} \times P(2)\big] \times Q_{\text{X}} \times (T \times \chi_{\text{obj}}^{\text{CF}}) \times N. \tag{A.7}$$

- Semi-continuous gold film
  In this case, $Q_{\text{XX}} = Q_{\text{X}}$, which leads to

$$I_{\text{tot}} = [P(1) + 2 \times P(2)] \times Q_{\text{X}} \times (T \times \chi_{\text{obj}}^{\text{SCF}}) \times N. \tag{A.8}$$

References

[1] Drexhage K H, Kuhn H and Schäfer F P 1968 Variation of the fluorescence decay time of a molecule in front of a mirror *Ber. Bunsenges. Phys. Chem.* **72** 329

[2] Lakowicz J R 2001 Radiative decay engineering: biophysical and biomedical applications *Anal. Biochem.* **298** 1–24

[3] Lakowicz J R 2005 Radiative decay engineering 5: metal-enhanced fluorescence and plasmon emission *Anal. Biochem.* **337** 171–94

[4] Akimov A V, Mukherjee A, Yu C L, Chang D E, Zibrov A S, Hemmer P R, Park H and Lukin M D 2007 Generation of single optical plasmons in metallic nanowires coupled to quantum dots *Nature* **450** 402–6

[5] Orrit M 2007 Nano-optics: quantum light switch *Nature Phys.* **3** 755–6

[6] Chang D E, Sorensen A S, Hemmer P R and Lukin M D 2006 Quantum optics with surface plasmons *Phys. Rev. Lett.* **97** 053002

[7] Schietinger S, Barth M, Aichele T and Benson O 2009 Plasmon-enhanced single photon emission from a nanoassembled metal–diamond hybrid structure at room temperature *Nano Lett.* **9** 1694–8

[8] Barthes J, Colas des Francs G, Bouhelier A, Weeber J C and Dereux A 2011 Purcell factor for a point-like dipolar emitter coupled to a two-dimensional plasmonic waveguide *Phys. Rev.* B **84** 073403
[9] Vion C, Spinicelli P, Coolen L, Schwob C, Frigerio J M, Hermier J P and Maitre A 2010 Controlled modification of single colloidal CdSe/ZnS nanocrystal fluorescence through interactions with a gold surface *Opt. Express* **18** 7440
[10] Purcell E M 1946 Spontaneous emission probabilities at radio frequencies *Phys. Rev.* **69** 681
[11] Gérard J M, Sermage B, Gayral B, Legrand B, Costard E and Thierry-Mieg V 1998 Enhanced spontaneous emission by quantum boxes in a monolithic optical microcavity *Phys. Rev. Lett.* **81** 1110
[12] Gayral B, Gérard J M, Sermage B, Lemaître A and Dupuis C 2001 Time-resolved probing of the Purcell effect for InAs quantum boxes in GaAs microdisks *Appl. Phys. Lett.* **78** 2828
[13] Laurent S, Varoutis S, Le Gratiet L, Lemaître A, Sagnes I, Raineri F, Levenson A, Robert-Philip I and Abram I 2005 Indistinguishable single photons from a single-quantum dot into a two-dimensional photonic crystal cavity *Appl. Phys. Lett.* **87** 163107
[14] Koenderink A F 2010 On the use of Purcell factors for plasmon antennas *Opt. Lett.* **35** 4208
[15] Maksymov I S, Besbes M, Hugonin J P, Yang J, Beveratos A, Sagnes I, Robert-Philip I and Lalane P 2010 Metal-coated nanocylinder cavity for broadband nonclassical light emission *Phys. Rev. Lett.* **105** 180502
[16] Song J H, Atay T, Shi S, Urabe H and Nurmikko A V 2005 Large enhancement of fluorescence efficiency from CdSe/ZnS quantum dots induced by resonant coupling to spatially controlled surface plasmons *Nano Lett.* **5** 1557
[17] Ito Y, Matsuda K and Kanemitsu Y 2007 Mechanism of photoluminescence enhancement in single semiconductor nanocrystals on metal surfaces *Phys. Rev.* B **75** 033309
[18] Matsuda K, Ito Y and Kanemitsu Y 2008 Photoluminescence enhancement and quenching of single CdSe/ZnS nanocrystals on metal surfaces dominated by plasmon resonant energy transfer *Appl. Phys. Lett.* **92** 211911
[19] Yuan C T, Pyng Yu, Ko H C, Huang J and Jau Tang 2009 Antibunching single-photon emission and blinking suppression of CdSe/ZnS quantum dots *ACS Nano* **3** 3051
[20] Mertens H, Koenderink A K and Polman A 2007 Plasmon-enhanced luminescence near noble-metal nanospheres: comparison of exact theory and an improved Gersten and Nitzan model *Phys. Rev.* B **76** 115123
[21] Mahler B, Spinicelli P, Buil S, Quélin X, Hermier J P and Dubertret B 2008 Towards non-blinking colloidal quantum dots *Nature Mater.* **7** 659
[22] Chen Y, Vela J, Htoon H, Casson J L, Werder D J, Bussian D A, Klimov V I and Hollingsworth J A 2008 'Giant' multishell CdSe nanocrystal quantum dots with suppressed blinking *J. Am. Chem. Soc.* **130** 5026
[23] Brokmann X, Hermier J P, Messin G, Desbiolles P, Bouchaud J P and Dahan M 2003 Statistical aging and nonergodicity in the fluorescence of single nanocrystals *Phys. Rev. Lett.* **90** 120601
[24] Spinicelli P, Buil S, Quélin X, Mahler B, Dubertret B and Hermier J P 2009 Bright and grey states in CdSe–CdS nanocrystals exhibiting strongly reduced blinking *Phys. Rev. Lett.* **102** 136801
[25] Wu X W, Gong M, Dong C H, Cui J M, Yang Y, Sun F W, Han Z F and Guo G C 2010 Anti-bunching and luminescence blinking suppression from plasmon-interacted single CdSe/ZnS quantum dot *Opt. Express* **18** 6340
[26] Ducourtieux S *et al* 2001 Near-field optical studies of semicontinuous metal films *Phys. Rev.* B **64** 165403
[27] Stockman M I, Faleev S V and Bergman D J 2001 Localization versus delocalization of surface plasmons in nanosystems: can one state have both characteristics? *Phys. Rev. Lett.* **87** 167401
[28] Grésillon S, Aigouy L, Boccara A C, Rivoal J, Quélin X, Desmarest C, Gadenne P, Shubin V A, Sarychev A K and Shalaev V M 1999 Experimental observation of localized optical excitations in random metal–dielectric films *Phys. Rev. Lett.* **82** 4520
[29] Raether H 1988 *Surface Plasmons on Smooth and Rough Surfaces and on Gratings* (*Springer Tracts in Modern Physics* vol. 111) (New York: Springer)

[30] Buil S, Aubineau J, Laverdant J and Quélin X 2006 Local field intensity enhancements on gold semicontinuous films investigated with an aperture nearfield optical microscope in collection mode *J. Appl. Phys.* **100** 063530

[31] Sanchez-Gil J A 2003 Localized surface-plasmon polaritons in disordered nanostuctured metal surfaces: shape versus Anderson-localized resonances *Phys. Rev.* B **68** 113410

[32] Krachmalnicoff V, Castanié E, De Wilde Y and Carminati R 2010 Fluctuations of the local density of states probe localized surface plasmons on disordered metal films *Phys. Rev. Lett.* **105** 183901

[33] Mallek-Zouari I, Buil S, Quélin X, Mahler B, Dubertret B and Hermier J P 2010 Plasmon assisted single photon emission of CdSe/CdS nanocrystals deposited on random gold film *Appl. Phys. Lett.* **97** 053109

[34] Gueroui Z and Libchaber A 2004 Single-molecule measurements of gold-quenched quantum dots *Phys. Rev. Lett.* **93** 166108

[35] Brokmann X, Coolen L, Hermier J P and Dahan M 2005 Emission properties of single CdSe/ZnS quantum dots close to a dielectric interface *Chem. Phys.* **318** 91

[36] Nair G, Zhao J and Bawendi M G 2011 Biexciton quantum yield of single semiconductor nanocrystals from photon statistics *Nano Lett.* **11** 1136